fire

MDPI

Article

Research on Fire Smoke Recognition Algorithm with Image Enhancement for Unconventional Scenarios in Under-Construction Nuclear Power Plants

Tingren Wang [1], Guangwei Liu [1], Kai Yu [2,*] and Baolin Yao [2]

[1] Zhangzhou Project Team, China Nuclear Engineering Co., Ltd., Zhangzhou 363300, China; wangtr@cnpe.cc (T.W.); liugw@cnpe.cc (G.L.)
[2] School of Safety and Environmental Engineering, Shandong University of Science and Technology, Qingdao 266590, China; m15634099737@163.com
* Correspondence: ykxfkd@sdust.edu.cn; Tel.: +86-13969849358

Abstract

Accurate identification of fire smoke is a key link in realizing early fire prevention and control. Traditional intelligent video and image processing technologies are significantly restricted by environmental factors, with weak anti-interference capabilities and limitations in distinguishing fire smoke, leading to a high false alarm rate of fires. To address this problem, this paper proposes an unconventional visual field smoke detection method based on image enhancement. The method innovatively improves the Retinex algorithm by integrating improved guided filtering, adaptive brightness correction, and CLAHE-WWGIF joint processing, which realizes targeted optimization for the unique interference factors of under-construction nuclear power plants such as water mist, low illumination, and equipment occlusion. First, an improved Retinex algorithm is used to process the image to improve the image brightness and contrast, retain edge details while avoiding halo artifacts, reduce the impact of noise, and optimize visual features. Then, the sample data set is integrated, and the YOLOv11 target detection algorithm is used to achieve accurate identification and positioning of smoke targets. Experimental data shows that the fire identification method achieves an accuracy rate of 93.6% and 92.3% for fire smoke identification in interference-prone scenarios such as dark nights and water mist, respectively, and the response time to fire smoke is only 1.8 s and 2.1 s. In practical on-site applications at nuclear power plant construction sites, the method is integrated into an "edge computing + distributed deployment" hardware system, which realizes real-time smoke detection in core areas such as nuclear islands and conventional islands with a false alarm rate of less than 5% and a detection delay of $\leq$300 ms, meeting the ultra-strict safety monitoring requirements of nuclear power projects. Experiments show that this method can be effectively applied to smoke detection scenarios under unconventional visual fields, accurately identify smoke, provide reliable technical support for fire smoke identification under unconventional visual fields, significantly reduce the false alarm rate of fire detection, and provide technical support for the safety of under-construction nuclear power plants.

Keywords: smoke detection; fire; image enhancement; YOLO; Retinex

Check for updates

Academic Editors: Haowei Yao, Xueming Shu, Xuecai Xie and Jun Hu

Received: 27 January 2026
Revised: 11 March 2026
Accepted: 16 March 2026
Published: 17 March 2026

Copyright: © 2026 by the authors. Licensee MDPI, Basel, Switzerland. This article is an open access article distributed under the terms and conditions of the Creative Commons Attribution (CC BY) license.

1. Introduction

Fire poses a great threat to projects under construction, especially nuclear power plant projects under construction, causing property damage and casualties. Fire prevention and

control play an important role in ensuring the smooth progress of projects [1–4]. Fires are accompanied by the generation of large amounts of smoke, and the rapid and effective identification of smoke is a key link in fire prevention and control work [5]. As a result, various smoke detection devices have been gradually developed and put into use.

Fire smoke detection methods usually rely on the color and texture features of images for identification [6,7]. Color feature-based methods have driven the development of various color space models. For example, Buriboev S et al. [8] proposed a model that combines deep learning with hybrid preprocessing methods such as contour-based algorithms and color feature analysis to provide reliable and accurate fire and smoke detection; Zhao L et al. [9] used a lightweight CNN model to study the impact of using infrared bands on early fire smoke detection in Landsat images; Ghali R et al. [10], using CT-Fire and DC-Fire models, utilized visible light and infrared aerial imagery to identify wildfires; Soocheol Kim et al. [11] proposed a smoke detection instrument that uses an LED array instead of an angle-positioned PD to measure multi-angle light scattering for smoke detection and classification based on multiple scattering; and Ghail R et al. [12] proposed a novel deep learning model, BoucaNet, for identifying smoke in satellite imagery while addressing the associated challenges.

The latest advancements in deep learning-based computer vision technologies (such as object detection and image segmentation) have demonstrated significant advantages in the field of industrial safety monitoring, and these technologies have also become important solutions for the early detection of fire smoke [13]. For example, Van Ha Hoang et al. [14] optimized the training hyperparameters of the YOLOv8 and YOLOv10 models using Bayesian tuning, which ultimately improved the detection performance of the models; Drzymała J et al. [15] proposed a real-time forest fire detection model based on YOLOv8, and established a fire dataset to verify the effectiveness and feasibility of the model; Ejaz et al. [16] proposed an architecture based on channel attention that can be used for fire detection, and experiments have shown that its channel attention mechanism has significant improvements compared to the baseline and state-of-the-art fire detection models; Xing Zhimin et al. [17] introduced a 3D convolutional spatiotemporal feature extraction module to capture the temporal dynamic features of flame flickering and smoke diffusion and identify fires; Pooja Verma et al. [18] developed a prototype depth monitoring unit (DSU) that employs a method to detect potential scenarios such as fires and issues alerts to users; Apostolopoulos Ioannis D et al. [19] proposed an Xception network, enhanced its post-explainability using Grad-CAM++ and LIME algorithms, and demonstrated, through experimentation, that it outperforms other convolutional neural networks, achieving remarkably high accuracy; Han Yu et al. [20] proposed a modular framework TriFireNet, which improved the accuracy of fire identification while reducing the computational cost; Samy et al. [21] used the machine learning algorithm YOLOv5 based on the computer vision model combined with an attention mechanism to identify and classify fires; Kawk et al. [22] employed a previously developed algorithm for dehazing, specifically the dark channel prior, to identify potential fire smoke areas, and experimental results confirmed its feasibility; and Chen et al. [23] proposed a forest fire detection model using multi-task learning. The normalized Wasserstein distance (NWD) was introduced to enhance the detection ability of small targets. However, various algorithms are often affected by environmental factors in practical applications, resulting in false alarms. There is still little research on fire identification in unconventional fields of view.

The environment for smoke identification in the construction area of nuclear power plants is typically complex, and the smoke targets to be identified exhibit multi-scale and dynamic diffusion characteristics. In engineering practice, although theoretically increasing the density of camera deployment can expand the monitoring coverage, nuclear power

plant construction areas are characterized by dense equipment and intersecting pipelines, making it difficult to install too many devices in some areas, and dense deployment would increase signal transmission and management costs. Furthermore, simply increasing the number of devices cannot solve the problem of environmental interference—low illumination (temporary nighttime lighting), high dust levels, and water mist from sprinkler trucks during construction can reduce the contrast between smoke and the background, even leading to visual confusion. Unlike civil construction, nuclear power plants have ultra-strict safety requirements for fire detection (ultra-low false alarm rate) and unique industrial interferences, which makes the proposed improved Retinex + YOLOv11 algorithm [24], with targeted anti-interference and multi-scale detection capabilities, far more adaptive than general civil smoke detection algorithms. In addition, smoke identification algorithms for nuclear power plants under construction need stronger anti-interference capabilities, particularly adaptability to uneven lighting, white interference (such as water mist), and equipment obstruction. This is crucial for achieving accurate smoke identification and reducing false alarm rates in unconventional field-of-view conditions. To achieve efficient smoke detection, a collaborative technical framework of "image preprocessing—target detection" needs to be constructed: first, image enhancement algorithms are used to eliminate environmental interference and highlight smoke features and then target detection algorithms are used to complete the accurate identification and localization of smoke. Among them, the image enhancement step is based on the Retinex algorithm and improved, while the target detection step needs to adapt to the characteristics of smoke "multi-scale and dynamic diffusion"—there is small local smoke in the gap between equipment and thin smoke in the distance at high altitude. Conventional single-scale detection algorithms are difficult to balance recognition accuracy and range. Therefore, the YOLO algorithm is introduced to form a complete technical solution of "improved Retinex + YOLOv11". Among them, YOLO is an end-to-end real-time object detection algorithm with outstanding performance in multi-scale target recognition and fast inference, which is suitable for the real-time smoke detection demand in the complex construction area of nuclear power plants.

This paper uses the trained YOLOv11 model to identify and locate smoke targets in images after image enhancement. The specific system flow is shown in Figure 1.

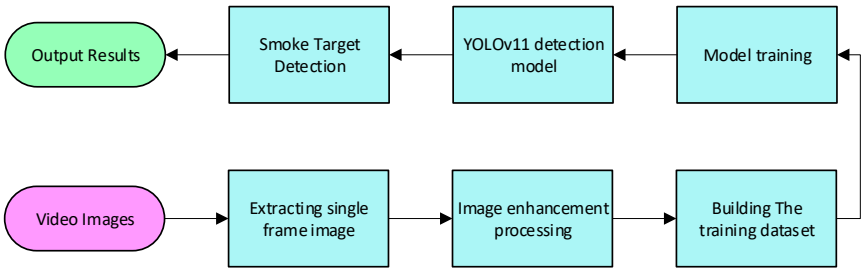


Figure 1. System flowchart.

This paper proposes a novel image-enhanced algorithm for identifying fire smoke in nuclear power plants under construction. This algorithm can effectively identify fire smoke generated in complex environments, reduce the impact of environmental factors on detection, and improve detection accuracy, thereby providing technical support for nuclear power plant projects under construction.

2. Materials and Methods

2.1. Dataset and Preprocessing

The experimental data in this paper comes from three sources: first, smoke video images from the fire video library of the CVPR laboratory at Keimyung University in

South Korea [25] (812 images, 23.6%); second, video images collected at the construction site of a nuclear power plant project (2224 images, 64.7%, including 1524 daytime images and 700 nighttime images); and third, images containing smoke targets collected from the Internet platform (401 images, 11.7%), which were filtered to be consistent with the industrial environment of nuclear power plant construction. A total of 3437 valid images were obtained after strict quality control. Then, the labelImg tool was used to label the smoke targets in all the images. Finally, the 3437 labeled images and 4 video images together constituted the experimental dataset. The labeled images were randomly divided into training sets and validation sets in an 8:2 ratio.

2.2. Methods

2.2.1. Improved Retinex Algorithm

First, the image is converted from the RGB color space to the HSV color space. For the luminance component in the HSV space, the improved multi-scale guided filtering algorithm is used to extract the illumination component. This process can effectively avoid the generation of halo artifacts while completely preserving the edge details of the image. Second, the extracted illumination component is subjected to adaptive luminance correction using the Weber–Fechner algorithm [26]. For the reflection component, the method of combining the contrast-limited adaptive histogram equalization (CLAHE) with the improved guided filtering is used to process it. This method can prevent the image from being over-enhanced and distorted and can also effectively suppress noise. Then, the corrected illumination component and the processed reflection component are fused using the principal component analysis method. Finally, in order to avoid color distortion in the image, the improved adaptive stretching method is used to perform color correction on the saturation component in the HSV space, and the luminance, saturation, and hue components are re-fused and converted back to the RGB color space to finally obtain the enhanced image. Its principal block diagram is shown in Figure 2.

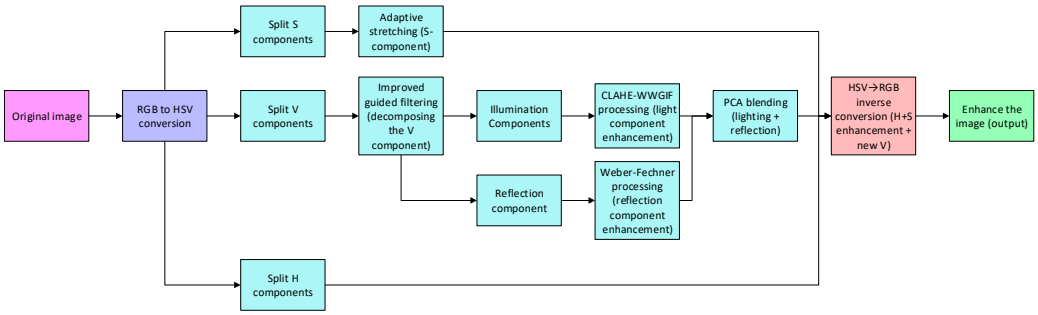


Figure 2. Improved Retinex.

Improved Guided Filtering Algorithm

Guided filtering is an edge-preserving, smoothing filtering algorithm proposed by Kaiming He et al. in 2010 [27]. Its core advantage lies in controlling the filtering process through the pixel information of the "guide image" (which can be the same as the input image or other related images). It can effectively smooth image noise, suppress redundant details, and accurately preserve edge and texture features. Its filtering result and the guide image are linearly correlated within the filtering window.

The coefficients are linearly fitted using the least squares method, and the cost function is expressed as:

$$E(a_k, b_k) = \sum_{i \in W_k} [(a_k I_i + b_k - p_i)^2 + \varepsilon {a_k}^2] \quad (1)$$

where $E(a_k, b_k)$ denotes the cost function of guided filtering for the k-th local window; a_k represents the linear gain coefficient of the k-th local window, which reflects the correlation

between the guide image and the input image; b_k is the linear offset coefficient of the k-th local window; i is the pixel index within the k-th local window; W_k stands for the k-th square local filtering window centered on the target pixel; I_i is the pixel gray value of the guide image at position i (the guide image is the same as the input image in this paper); p_i denotes the pixel gray value of the input image at position i; and ε is a positive regularization parameter to prevent a_k from being too large, with a fixed value of 0.01 in this experiment.

Weighted guided filtering (WGIF), within the framework of guided filtering (GIF), adds an edge weight factor to achieve adaptive adjustment of the regularization parameter. While this optimization alleviates the halo blurring problem at image boundaries, its edge-aware factor relies on the local window variance definition, which has two limitations: First, regions with high variance are not necessarily edge regions; second, it lacks sensitivity to weak edge regions. Incorporating gradient information into the edge-aware weights can enhance the ability to identify weak edges and further improve the algorithm's robustness. Therefore, the proposed new edge weight factor is expressed as:

$$\Gamma_1(k) = \frac{1}{N}\sum_{i=1}^{N} \frac{\sigma_{1.1}^2(k)\sigma_{1,\mathrm{r}}^2(k) + G(\sqrt{k_x^2 + k_y^2}) + (0.001 \times l)^2}{\sigma_{1.1}^2(i)\sigma_{1,\mathrm{r}}^2(i) + G(\sqrt{i_x^2 + i_y^2}) + (0.001 \times l)^2} \tag{2}$$

where $\Gamma_1(k)$ is the new edge weight factor of the k-th local window; N is the total number of pixels in the local filtering window; $\sigma_{1.1}^2(k)$ and $\sigma_{1,\mathrm{r}}^2(k)$ represent the variance of the guide image in the k-th local window at different scales; $\sigma_{1.1}^2(i)$ and $\sigma_{1,\mathrm{r}}^2(i)$ are the variances of the guide image at pixel i in the k-th local window at different scales; G$(\cdot)$ denotes the Gaussian filter function for smoothing gradient information; k_x and k_y are the gradient values of the central pixel of the k-th window in the x and y directions, respectively; i_x and i_y are the gradient values of pixel i in the x and y directions, respectively; and l is the dynamic range of the input image, with a value consistent with the maximum gray value of the input image (255 for 8-bit images).

As shown in Equation (3), the filtering effect of the output image is determined by the window coefficient a_k: When $a_k = 1$, it indicates that the image is in an edge region and that the region is well preserved; when $a_k = 0$, it indicates that the image is in a flat region and the smoothing effect is good. However, WGIF lacks explicit edge constraints, resulting in the inability to effectively preserve edges. In order to preserve edges, while taking into account the weak details in flat regions, a new edge protection constraint is proposed as:

$$\gamma_k = \frac{1}{1 + e^{-\sqrt{k_x^2 + k_y^2}}} \tag{3}$$

When located in the edge region, γ_k approaches 1; when located in the flat region, γ_k approaches 0. The new cost function is expressed as:

$$E(a_k, b_k) = \sum_{i \in w_k} [(a_k I_i + b_k - p_i)^2 + \frac{\varepsilon}{\Gamma_1(k)}(a_k - \gamma_k)^2] \tag{4}$$

where all parameters $E(a_k, b_k)$, a_k, b_k, i, I_i, p_i, ε are consistent with the definitions in Formula (1); w_k is the k-th local filtering window (same as W_k in Formula (1)); $\Gamma_1(k)$ is the edge weight factor in Formula (2); and γ_k is the edge protection constraint factor in Formula (3). The improved cost function adds an edge constraint term based on the original guided filtering, which realizes the adaptive adjustment of regularization parameters according to edge information.

By improving the guided filtering algorithm, the halo blurring problem at image boundaries under unconventional fields of view can be alleviated, reducing the resulting false alarm problem. At the same time, by incorporating gradient information into edge perception weights, the ability to identify weak edges can be strengthened, further improving the robustness of the fire smoke identification algorithm.

Enhancement and Extraction of Light Components

To address the limitations of Gaussian filtering in the Retinex algorithm, an improved guided filtering algorithm is used instead of Gaussian filtering in the illumination component extraction stage, combined with multi-scale weighted processing. This scheme not only effectively avoids halo blurring but also largely preserves the edge features and details of the original input image. The illumination components are represented as:

$$L_1(x,y) = \sum_{n=1}^{N} w_n[q_n(x,y) * I(x,y)] \tag{5}$$

where $L_1(x,y)$ denotes the illumination component value of the image at pixel position (x,y) after multi-scale guided filtering; n is the scale index of the multi-scale guided filter; N is the total number of scales, with a fixed value of 3 in this paper (small, medium, and large scales); w_n is the weight coefficient of the n-th scale, with $w_1 = w_2 = w_3 = 1/3$ (equal weight for each scale); $q_n(x,y)$ is the improved guided filter function at the n-th scale; $*$ represents the convolution operation; and $I(x,y)$ is the pixel gray value of the input image at position (x,y).

The Weber–Fechner law [28] is a key formula in psychophysics that describes the relationship between the intensity of human perception and the intensity of external environmental stimuli. In the dimension of light intensity change, it can be used to show that there is a logarithmic linear relationship between the degree of a human eye's perception of light intensity change and the initial light intensity. Considering that there is still room for improvement in the visual quality and perception effect of the image after obtaining the estimated illumination component, it is necessary to enhance the illumination component. Based on the core principle of the above law, the brightness enhancement method proposed in this paper is as follows: by means of adaptive adjustment of the bright and dark areas of the image, it can not only improve the overall quality of the image with uneven illumination but also retain the details of the original image to a certain extent. The output image is represented as:

$$L_{out} = \lambda \lg L_{in} + \lambda_0 \tag{6}$$

where $\boldsymbol{L_{out}}$ is the brightness-enhanced illumination component pixel value; $\boldsymbol{\lambda}$ is the brightness adjustment coefficient, a positive constant with a value of 0.8 in this experiment to avoid over-enhancement; $\lg(\cdot)$ is the common logarithm function; $\boldsymbol{L_{in}}$ is the original illumination component pixel value before enhancement (i.e., $\boldsymbol{L_1(x,y)}$ in Formula (5)); and $\boldsymbol{\lambda_0}$ is the Weber constant, a fixed offset constant with a value of 1.0 to ensure the pixel value is within a valid range.

Enhanced Reflection Component

Contrast-limited adaptive histogram equalization (CLAHE) [29] based on histogram equalization improves image smoothness by incorporating interpolation. While preserving image details and features and limiting excessive contrast amplification in local smooth areas, this algorithm still has the limitation of not being able to completely suppress noise. In contrast, the WWGIF filtering algorithm has the dual ability to restore image details and

reduce noise. Therefore, this paper proposes a new algorithm called CLAHE-WWGIF to process the reflection component. This algorithm can further weaken the negative impact of noise while improving image contrast and preserving details.

Since the noise is mainly concentrated in the reflection component of the image, even if the CLAHE algorithm is used to process the image, this part of the noise is still difficult to eliminate. Therefore, the WWGIF filtering operation needs to be applied to the image after CLAHE processing. While maintaining the advantage of CLAHE in improving image contrast, the residual noise is effectively suppressed, and the overall image quality is optimized. The guided image is represented as:

$$R(i) = \overline{a_i} R'(i) + \overline{b_i} \tag{7}$$

where $R'(i)$ is the pixel value of the reflection component at position i after CLAHE-WWGIF joint processing; $\overline{a_i}$ is the average value of the linear gain coefficient a_k in the local window centered on pixel i (consistent with the definition of a_k in Formula (1)); $R'(i)$ is the pixel value of the reflection component at position i after contrast enhancement with the CLAHE algorithm; and $\overline{b_i}$ is the average value of the linear offset coefficient b_k in the local window centered on pixel i (consistent with the definition of b_k in Formula (1)).

Saturation Component Processing

In the HSV color space, the saturation component is a key element determining the overall color visual presentation of an image. When enhancing low-light images, the increase in brightness often leads to a corresponding change in saturation. Processing only the brightness component can easily cause color distortion and insufficient saturation, resulting in an overexposed appearance that does not conform to normal human visual perception. Therefore, the stretched image is represented as:

$$S_{out} = \frac{S_{in} - L}{H - L} \tag{8}$$

where S_{out} is the saturation component pixel value after adaptive stretching and correction; S_{in} is the original saturation component pixel value of the input image at the target position (in HSV color space); L is the lower limit of saturation component stretching, with a fixed value of 0 (the minimum value of saturation component in HSV space); and H is the upper limit of saturation component stretching, with a fixed value of 1 (the maximum value of the saturation component in HSV space). The formula realizes the normalized stretching of the saturation component to avoid color distortion caused by brightness enhancement.

An improved Retinex algorithm was applied for image enhancement of multi-type interference targets that are easily misrecognized as fire smoke in the construction area of nuclear power plants—this misrecognition is the primary cause of the high false alarm rate of traditional smoke detection algorithms in unconventional scenarios. Figure 3a shows the original images of typical interference targets collected from key construction areas (pipeline flushing zone, welding zone, and mechanical operation zone) of nuclear power plants, including water jet/water mist from sprinkler trucks, floating construction dust, dark equipment shadows caused by dense pipelines, and strong light reflections on metal equipment surfaces. In the unenhanced original images, these interference targets exhibit fuzzy visual features, low contrast with the background, and high similarity with fire smoke (e.g., the white diffusion state of water mist and dust is highly consistent with smoke, and the dark block of equipment shadow is easily mistaken for thick smoke), leading to the failure of traditional detection algorithms to effectively distinguish smoke from interference targets.

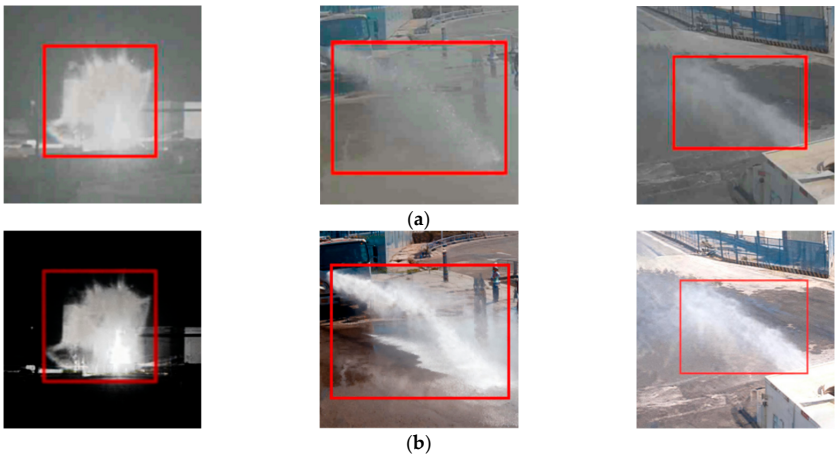


Figure 3. Image enhancement results of typical interference targets in under-construction nuclear power plants via improved Retinex algorithm (The content within the red box is misrecognized interference factors). (**a**) Original images of multi-type interference targets in nuclear power plant construction areas. (**b**) Enhanced images after processing by the improved Retinex algorithm.

Figure 3b shows the enhanced images of the above interference targets processed by the improved Retinex algorithm in this paper. The algorithm significantly improves the brightness and contrast of the original images, effectively preserves the unique edge, texture and shape features of each interference target while avoiding halo artifacts, and suppresses the noise interference of dust and strong light reflection. Specifically, (1) water jet/water mist presents a continuous, directional flow texture with clear boundary edges after enhancement; (2) construction dust shows a discrete, floating particle feature with uneven light reflection; (3) equipment shadows exhibit a fixed shape consistent with the equipment outline with sharp edge boundaries; and (4) strong light reflection shows a high-brightness specular feature with an obvious light and shade gradient. In contrast, fire smoke has inherent features of diffusion, irregular diffusion, and fuzzy edge contours that are completely different from the above interference targets.

By highlighting the differentiated visual features between various interference targets and fire smoke, the improved Retinex algorithm effectively eliminates the visual confusion between interference sources and smoke targets. This makes the subsequent YOLOv11 target detection algorithm able to accurately extract and identify the feature information of smoke and interference targets, significantly improving the accuracy of smoke target cropping and recognition, and fundamentally reducing the false alarm rate caused by the misrecognition of interference targets as smoke in nuclear power plant construction scenarios.

To further quantify the performance of the improved Retinex algorithm in enhancing false recognition target images and its contribution to smoke detection accuracy and false alarm rate reduction, six core evaluation indicators closely related to the distinction between false recognition targets and fire smoke were selected to compare the scheme without image enhancement (original images directly input into YOLOv11) and the scheme with improved Retinex image enhancement (enhanced images input into YOLOv11), as shown in Table 1. All experimental data are the average values of multiple tests on the four types of false recognition target images in Figure 3, ensuring the objectivity and reliability of the results.

Table 1. Quantitative comparison of schemes with/without improved Retinex image enhancement.

Index	CR	EPI	NSR/%	TCI	FDI	FRR/%
Original Image	10.5	0.56	58.3	0.52	0.38	23.5
Enhanced Image	41.8	0.96	96.7	0.94	0.91	2.5

2.2.2. Smoke Monitoring Baseline Model

The improvements in this paper are based on the YOLOv11 model of the YOLO series, and the model is optimized for the multi-scale smoke characteristics and unconventional field of view in nuclear power plant construction. YOLOv11 is an advanced real-time object detection model developed by the Ultralytics team. It has been continuously optimized and upgraded on the basis of the YOLO series algorithm [30]. The model adopts a C2f feature fusion module with a more lightweight hierarchical structure. This module realizes the efficient fusion of shallow detailed features and deep semantic features by adding branch connections. It is more suitable for extracting multi-scale smoke features in nuclear power plant construction scenarios. These features include small smoke in equipment gaps and thin smoke at high altitude. One of the core improvements of this algorithm is the anchor-free detection paradigm. This paradigm abandons the predefined anchor box and directly predicts the target bounding box through the key point regression method. It reduces the model complexity and improves the detection speed of irregularly diffused smoke targets. In addition, YOLOv11 designs a multi-scale detection head with adaptive receptive field. This detection head covers small, medium and large scales. It can automatically adjust the feature extraction range according to the smoke target size. It effectively solves the problem of low detection accuracy of small and medium smoke targets in complex construction environments. Specifically, the algorithm first obtains feature maps of three different depths. In order to achieve an effective combination of multi-scale features, YOLOv11 adopts an enhanced feature fusion structure based on the C2f module and spatial pyramid pooling. This structure realizes full fusion and utilization of multi-scale features without relying on the traditional feature pyramid network (FPN) in the early versions. In the target localization stage, YOLOv11 abandons the traditional anchor-based mechanism and adopts an anchor-free detection paradigm, which directly predicts the position and size of the target without relying on predefined anchor boxes. During model training, the algorithm constructs a loss function with the intersection-over-union (IoU) between the predicted bounding box and the ground truth bounding box as the core metric. The model parameters are then continuously updated using the training set, enabling the model to accurately locate the target and determine its specific range in the original image. This paper uses the YOLOv11 method to identify and locate smoke targets using the trained model.

3. Results

To comprehensively evaluate the performance of the proposed smoke detection method, standard evaluation metrics including *Precision*, *Recall*, *F*1-score, Mean Average Precision (*mAP*), and false positive rate (*FPR*) are adopted together with the overall accuracy (*Accr*). The specific calculation formulas and parameter definitions of these metrics are as follows:

$$Precision = \frac{TP}{TP + FP}$$

$$Recall = \frac{TP}{TP + FN}$$

$$F1 - score = 2 \times \frac{Precision \times Recall}{Precision + Recall}$$

$$mAP = \frac{1}{N}\sum_{i=1}^{N} AP_i$$

$$FPR = \frac{FP}{FP + TN}$$

$$Accr = \frac{TP + TN}{TP + FP + TN + FN}$$

where TP (True Positive) denotes the number of correctly detected smoke targets; FP (false positive) denotes non-smoke targets incorrectly detected as smoke (false alarms); FN (False Negative) denotes smoke targets not detected (missed detections); TN (True Negative) denotes non-smoke targets correctly identified; N denotes the number of target categories (only smoke in this study); and AP_i denotes the Average Precision of the smoke category. In addition, the Precision–Recall (PR) curve is plotted to reflect the trade-off between the Precision and Recall of the model under different interference scenarios, and the curve results verify the stable detection performance of the proposed method.

3.1. Experimental Dataset

The experimental data in this paper comes from three sources: (1) smoke video images from the fire video library of the CVPR laboratory at Keimyung University in South Korea [25] (812 images, 23.6%); (2) video images collected at the construction site of a nuclear power plant project (2224 images, 64.7%, including 1524 daytime images and 700 nighttime images); and (3) images containing smoke targets collected from the Internet (401 images, 11.7%), which were filtered to match the actual environment of nuclear power plant construction. A total of 3437 valid smoke images were screened and retained after strict quality control, removing blurry, severely occluded, and low-quality samples. Although the dataset scale is not extremely large, it covers all typical on-site interference scenarios (daytime, nighttime, water mist, dust, and equipment occlusion) of nuclear power plant construction, which can fully support the verification of the effectiveness and feasibility of the proposed algorithm. Then, the labelImg tool was used to label the smoke targets in all of the images. Finally, the 3437 labeled images and four video images together constituted the experimental dataset. The labeled images were randomly divided into training and validation sets in an 8:2 ratio (2750 training images and 687 validation images). During the experiment. The official YOLOv11 pre-trained weights trained on the COCO dataset were introduced. Transfer learning was used to adjust the parameters of the new model to accelerate the convergence speed of the model. The initial learning rate of the model was set to 0.001, and the learning rate update strategy adopted cosine annealing. The batch size was set to four. After 50 epochs of training, the model loss value gradually stabilized.

3.2. Experimental Environment and Results

The configuration used in this experiment was the Windows 11 operating system, 16 GB memory, NVIDIA RTX3060 GPU (manufactured by NVIDIA Corporation, Santa Clara, CA, USA), and Intel Core i5 CPU (manufactured by Intel Corporation, Santa Clara, CA, USA); the software platform included deep learning framework PyTorch 1.7.0 and Python 3.8.

3.2.1. Comparative Experiment

The method presented in this paper is used to identify smoke videos (artificially simulated) collected from the construction site of a nuclear power plant project containing interference factors (sprinkler operation, nighttime lighting, dust, etc.), and compare them with the improved SSD smoke detection algorithm [31], GMM Gaussian mixture model method [32], and YOLOv11 detection model. The experimental results of the method presented in this paper for smoke video images are shown in Table 2, where Accr is the detection accuracy, that is, the percentage of the number of smoke target frames detected to the number of smoke target frames in the video image.

The detection results of each method are shown in Table 3. Compared with other methods, this method has good performance in the detection and recognition of smoke in unconventional fields of view.

Table 2. Experimental results of smoke video images.

Video	Frames	Experimental Results		Evaluation Index
		First Detected Target Frame	Number of Detected Target Frames	Accr/%
Smoke Video 1	368	6	337	91.58
Smoke Video 2	679	34	643	94.70
Smoke Video 3	2144	71	1947	90.81
Smoke Video 4	1503	48	1452	96.61
Average	1174	40	1095	93.27

Table 3. Comparison of smoke detection results.

Algorithm Name	Accr/%	FPS/(f/s)	Precision/%	Recall/%	F1-Score/%	mAP@0.5/%	FDR/%
Gaussian mixture model (GMM)	92.11	35.24	88.3	89.5	88.8	87.3	12.9
Improved SSD smoke detection algorithm	91.34	42.73	90.5	88.9	89.7	88.5	8.7
YOLO detection model	86.25	47.98	91.8	85.7	90.7	90.1	7.2
The model in this paper	94.07	38.62	94.2	91.8	93.0	92.7	4.5

To further realize the systematic evaluation of the false positive rate (FPR) in comparative experiments, the FPR values of each algorithm under the same nuclear power plant construction interference scenarios (water mist, nighttime, and dust) are tested and counted. The results show that the proposed method achieves an average FPR of 4.5% in comparative experiments, which is significantly lower than the Gaussian mixture model (12.9%), improved SSD (8.7%), and the general YOLOv11 model (7.2%). Meanwhile, the proposed method achieves a Precision of 94.2%, Recall of 91.8%, F1-score of 93.0%, and mAP@0.5 of 92.7% on the constructed dataset (Figure 4), which outperforms other comparison algorithms in all standard evaluation indicators, fully verifying the superiority of the proposed method in detection accuracy and anti-interference ability.

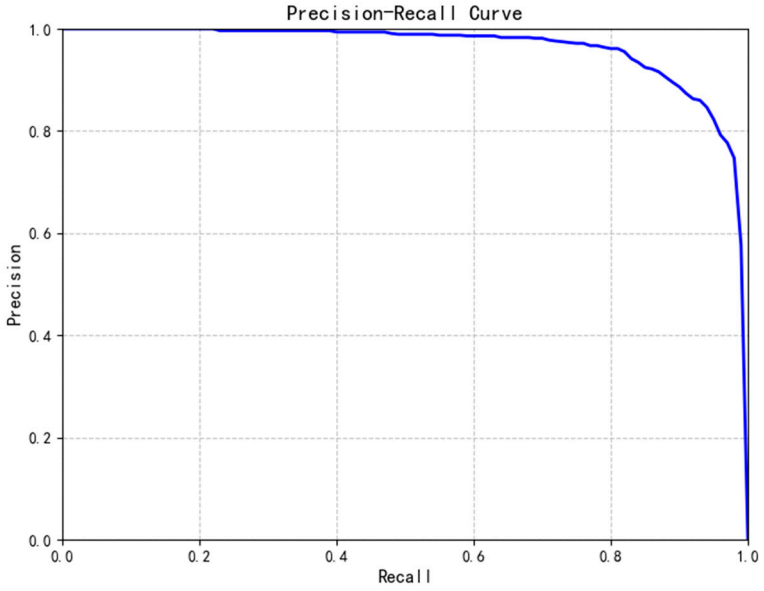


Figure 4. The Precision–Recall curve of the model in this paper.

Compared with other methods, this method has good performance in the detection and recognition of smoke in unconventional fields of view. The experimental results in the table show that the proposed method performs well in identifying fire smoke in unconventional

areas of nuclear power plants under construction. It achieves higher detection accuracy for smoke targets while maintaining a high detection speed. Its overall performance surpasses other static or dynamic target detection methods, demonstrating greater applicability in smoke target detection tasks within unconventional areas. In practical scenario comparison, the GMM and improved SSD algorithms show obvious performance degradation in high-interference scenes such as nuclear power plant water mist and nighttime welding, while the proposed model maintains a low false alarm rate due to the adoption of a targeted image enhancement module. In addition, compared with the general YOLOv11 model, this method has better adaptability to small smoke targets in equipment gaps and thin smoke at high altitudes, which is more in line with the actual detection needs of nuclear power plant construction sites.

3.2.2. Ablation Experiment

Table 4 presents the ablation experiment results. As shown in Table 4, when all three improvement measures mentioned in Section 2.2.1 are adopted, the model exhibits the best performance in recognizing smoke targets in unconventional fields of view, achieving a maximum accuracy of 94.52. The above ablation experiment results demonstrate that the improvement measures have a significant effect on performance enhancement.

Table 4. Ablation experiment results.

EIC	ERC	PSC	Accr/%	FPS/(f/s)	Precision/%	Recall/%	F1-Score/%	mAP@0.5/%	FDR/%
—	—	—	88.92	46.38	86.1	84.5	85.3	83.2	9.8
√	—	—	89.47	41.23	85.8	86.2	86.0	83.9	9.2
—	√	—	90.02	44.59	87.3	85.4	86.3	84.4	8.6
—	—	√	90.74	43.35	88.2	85.9	87	85.1	8.0
√	√	—	91.18	40.07	88.5	87.1	87.8	85.8	7.4
√	—	√	90.23	39.50	87.6	85.7	86.6	84.6	8.8
—	√	√	91.33	42.79	88.9	87.3	88.1	86.2	7.1
√	√	√	94.07	38.62	94.2	91.8	93.0	92.7	4.5

4. Discussion

4.1. System Application in Under-Construction Nuclear Power Plants

4.1.1. Application Scenario Adaptation

Construction areas of nuclear power plants under construction present complex environmental characteristics [33], including dense equipment, crisscrossing pipelines, variable lighting (such as plant shadows and nighttime construction lighting), and dust interference. Conventional detection systems are prone to misjudgment due to obstruction or ambient light. The smoke detection algorithm proposed in this study, through an improved Retinex image enhancement module, can effectively handle low-light, high-dust images in construction scenarios, eliminating the interference of equipment shadows and strong light halos on smoke recognition. The YOLOv11 multi-scale feature fusion capability can accurately identify smoke targets at different distances, including local smoke between close-range equipment gaps and thin smoke spreading at high altitudes at long distances, adapting to the detection needs of core construction areas such as the nuclear island, conventional island, and auxiliary buildings.

4.1.2. System Hardware Deployment Scheme

Based on the characteristics of the nuclear power plant under construction [34], the system adopts a hardware architecture of "edge computing + distributed deployment," with the following specific configuration:

1. Front-end Perception Layer: Network cameras with high-definition night vision capabilities are deployed at key locations in the construction area (such as cable trays, oil depots, and welding work areas). These cameras support real-time acquisition at 1080 P resolution with a frame rate $\geq$ 25 fps, meeting the algorithm's requirements for image quality and real-time performance. The cameras have built-in temperature sensors to help eliminate interference from high-temperature equipment (such as welding machines) in smoke detection.

2. Edge Computing Layer: Edge computing terminals (equipped with Intel i7 CPUs, manufactured by Intel Corporation, Santa Clara, CA, USA, and RTX3050 GPUs, manufactured by NVIDIA Corporation, Santa Clara, CA, USA) are deployed in each construction zone, embedding the improved smoke detection algorithm into the terminals. Image data collected by the front-end cameras is transmitted to the edge terminals in real time. The terminals perform image enhancement, smoke recognition, and localization calculations. A single terminal can process data streams from eight cameras simultaneously, with a detection latency $\leq$ 300 ms, meeting the real-time early warning requirements on-site.

3. Data Transmission Layer: A combination of industrial Ethernet and a 5G private network is used for transmission. Edge terminals transmit detection results (including smoke location, confidence level, and real-time images) to the central control platform. For signal-shielded areas such as the nuclear island, wireless repeaters are used to enhance the signal and ensure data transmission stability, with a packet loss rate $\leq$ 0.1%.

4. Central Control Management Layer: Monitoring servers and display terminals are deployed in the nuclear power plant construction control center. The server receives data from each edge terminal, constructs a visual monitoring interface, and displays the smoke detection status of each monitoring point in real time. When smoke is detected, the system automatically triggers an audible and visual alarm, marks the smoke location on the interface, and simultaneously pushes a warning message to the mobile app of on-site management personnel.

4.1.3. Field Experiment and Application Results

Field Experiment Design

The field experiments were conducted on a typical under-construction nuclear power plant located in southeastern China. The plant is a large-scale commercial nuclear power project under normal construction, including the conventional island, nuclear island auxiliary areas, pipeline installation zones, and welding operation areas. Due to construction safety and confidentiality requirements, detailed geographic coordinates and specific project names are not disclosed in this paper, but the experimental scenarios, equipment layout, and environmental interference characteristics are all consistent with the actual construction conditions of nuclear power plants. To address interference scenarios such as long-range spotlights at night and water mist from sprinkler trucks, a 15-day special experiment was conducted in the main core construction area of a nuclear power plant under construction. The experiment's plan is shown in Table 5.

Table 5. On-site experiment plan.

Experimental Scenario	Experiment Duration	Number of Testing Points	Interference Factors
Welding work area	15 days	8	Welding sparks, equipment shielding, dust
Auxiliary plant oil depot area	15 days	4	Strong light reflection, ventilation airflow
Nighttime welding area	15 days	8	Temporary lighting direct light/shadow, welding sparks, nighttime dust
Conventional island pipeline flushing area	15 days	8	Water spray from sprinkler trucks, strong light reflection, and ventilation airflow

During the test, a real interference scenario was constructed by using a smoke generator (simulating cable overheating and oil leakage smoke) and the standard operating procedure of a water truck. The system detection results and manual observation results were recorded simultaneously to verify the performance of the algorithm under specific interference.

Application Effect Verification

Field application results demonstrate that the system exhibits excellent detection performance in scenarios susceptible to interference, such as nighttime operation and water truck operations. Key performance indicators are as follows:

Nighttime Detection Performance: The smoke detection accuracy in the nuclear island's nighttime welding area reaches 93.6%, with a 91.2% accuracy rate for mid-to-long-range smoke (10–20 m from the camera) and a 95.8% accuracy rate for near-range smoke (within 5 m of equipment gaps).

Water Mist Interference Detection Performance: The system achieves a 92.3% accuracy rate in distinguishing between smoke and water mist in the conventional island's pipeline flushing area. It achieves an 89.7% accuracy rate for diffused smoke affected by airflow, and a false positive rate of only 4.1% for water mist, significantly outperforming traditional smoke detection algorithms.

Real-time Response and Stability: In nighttime scenarios, the system's average response time from smoke appearance to alarm is 2.1 s; in water mist scenarios, the average response time is 1.8 s, both meeting the time requirements for emergency response in nuclear power plants under construction. During the 15-day testing period, the system experienced no hardware failures or data interruptions. This stable performance in nuclear power plant scenarios also verifies its good transferability to other industrial high-interference scenarios such as chemical industrial parks and tunnel construction, where it outperforms traditional smoke detection algorithms in adapting to dust, strong light, and equipment occlusion compared with civil construction detection schemes.

The on-site experimental data and application effects in Section 4.1 fully verify the feasibility of the proposed algorithm in practical nuclear power plant construction scenarios. The following section will further analyze the core performance advantages and innovative value of the algorithm in addressing unconventional field-of-view smoke detection problems.

4.2. Algorithm Performance and Innovation Analysis

Current research on smoke recognition in nuclear power plant fires under construction largely focuses on algorithm applications within conventional visual domains, with less attention paid to unconventional visual domains during construction (such as dense equipment obstruction, complex lighting, and water mist). This study aims to propose an improved Retinex algorithm to address the problem of feature blurring in smoke images due to environmental interference in such scenarios. The algorithm is hypothesized to effectively enhance the contrast between smoke and the background, highlighting smoke features. Results show that the visual quality of smoke images is significantly improved after processing with the improved Retinex, laying a solid foundation for subsequent smoke recognition. In low-light scenarios at nuclear power plants, the improved Retinex effectively solves the halo and weak edge loss problems of the traditional Retinex algorithm by optimizing illumination component extraction and brightness correction. For example, after processing, the edge contour clarity of smoke images from nighttime construction areas is significantly improved, and the texture and other detailed features of the smoke are more easily captured by the recognition algorithm. The results demonstrate that the

improved Retinex algorithm effectively achieves the goal of enhancing smoke image features, providing strong support for accurate smoke recognition. Based on the above analysis of the algorithm's performance enhancement mechanism, this section summarizes the current research limitations and outlines the future optimizations direction to further expand the algorithm's application scope.

4.3. Research Limitations and Future Prospects

While this study's dataset covers various nuclear power plant construction scenarios, there is still room for improvement in sample coverage for some highly specialized working conditions. However, the existing samples are sufficient to support the effectiveness verification of the improved Retinex algorithm. Subsequent research will also add more comparative experiments with civil smoke detection algorithms in actual complex scenes to further quantify the adaptability difference between the proposed algorithm and general algorithms in different application scenarios. Further research can enrich the dataset and incorporate more diverse recognition algorithms to conduct in-depth studies on the entire process from image enhancement to final smoke recognition, thus more comprehensively verifying the algorithm's application effects in real-world scenarios.

The improved Retinex algorithm proposed in this study provides a new approach to image enhancement in unconventional viewpoints, enriches the application and optimization theory of the Retinex algorithm in industrial scenarios, and provides a reference for subsequent related algorithm research. Furthermore, this algorithm can preprocess smoke images collected in the construction area of a nuclear power plant under construction, improving image quality, aiding in subsequent smoke recognition, providing early warning of fire smoke, and reducing fire risks. Its adaptability to complex environments can also be extended to image preprocessing in other industrial scenarios (such as chemical industrial parks and tunnel construction), providing technical support for safety monitoring and other applications in these scenarios.

5. Conclusions

This paper addresses the problems of traditional smoke detection techniques, such as high false alarm rates due to environmental interference in unconventional visual fields and difficulty in accurately identifying smoke from fires at nuclear power plants under construction. A smoke detection method based on improved Retinex image enhancement and YOLOv11 is proposed. First, the improved Retinex algorithm is used to process the image, converting it from RGB to HSV space. Then, an improved guided filter is used to extract the illumination component, the Weber–Fechner algorithm is used to correct the brightness, the CLAHE-WWGIF algorithm is used to process the reflection component, and the saturation component is corrected before converting back to RGB space to optimize visual features. The core innovations of this study are twofold: First, the Retinex algorithm is innovatively optimized for the unique interference characteristics of under-construction nuclear power plants (water mist, low illumination, and equipment occlusion), including an improved guided filter with gradient information and edge protection constraints to eliminate halo artifacts, adaptive brightness correction based on the Weber–Fechner law for uneven lighting, and a CLAHE-WWGIF joint algorithm for the dual optimization of contrast enhancement and noise suppression, which effectively distinguishes smoke from white interference; second, a targeted technical framework of "improved Retinex + YOLOv11" is constructed, combining image enhancement for interference elimination with multi-scale feature fusion for smoke detection, making up for the deficiency of single algorithms in anti-interference and multi-scale target recognition in nuclear power plant construction scenarios. Subsequently, multi-source datasets are integrated, and YOLOv11 is used to fuse

multi-scale features to achieve the accurate identification and localization of smoke targets. Experimental results show that this method has a high average detection accuracy and outperforms methods such as Gaussian mixture model (GMM) and improved SSD, making it more suitable for smoke detection scenarios in unconventional visual fields.

The methodology of this research will be continuously iterated and optimized from multiple dimensions: On the one hand, the extreme scenario samples will be systematically expanded to cover the typical complex operating conditions of nuclear power plants under construction, such as strong backlight, high dust, and dense equipment obstruction. By constructing a dynamic dataset, the robustness of the model in edge scenarios will be further improved. On the other hand, the algorithm structure will be deeply optimized, and a lightweight network architecture design and model pruning techniques will be adopted to further compress the number of model parameters while ensuring detection accuracy, thereby achieving the lightweight deployment of embedded equipment in nuclear power plants. At the same time, the research results will be extended to other industrial high-interference fire detection scenarios (e.g., chemical industrial parks, tunnel construction), enriching the application system of image enhancement-based smoke detection algorithms and providing a technical reference for the intelligent upgrade of industrial fire safety monitoring. At the same time, the integration of multimodal data such as infrared thermal imaging and gas sensors will be explored to overcome the limitations of single visual detection and construct a "vision-multi-sensor" fusion fire early warning system for nuclear power plants under construction. This will enable the intelligent early warning of fires across the entire chain, providing more reliable and comprehensive technical support for fire safety in nuclear power plant projects.

Author Contributions: Conceptualization and methodology, T.W. and K.Y.; software, validation, and formal analysis, G.L. and B.Y. All authors have read and agreed to the published version of the manuscript.

Funding: This research received no external funding.

Data Availability Statement: The original contributions presented in this study are included in the article. Further inquiries can be directed to the corresponding author.

Acknowledgments: Thanks to authors for their efforts in this research.

Conflicts of Interest: Author Tingren Wang and Guangwei Liu were employed by the company Zhangzhou Project Team, China Nuclear Power Engineering Co., Ltd. The remaining authors declare that the research was conducted in the absence of any commercial or financial relationships that could be construed as a potential conflict of interest.

Abbreviations

The following abbreviations are used in this manuscript:

YOLO	You Only Look Once
CR	Contrast Ratio
EPI	Edge Preservation Index
NSR	Noise Suppression Ratio
TCI	Texture Clarity Index
FDI	Feature Distinction Index
FRR	False Recognition Rate
EIC	Enhancement and Extraction of Light Components
ERC	Enhanced Reflection Component
PSC	Processing of Saturation Component
FPS	Frames Per Second

References

1. Mambile, C.; Leo, J.; Kaijage, S. Deep Learning Models for Forest Fire Prediction: Insights into Feature Selection for Climate-Resilient Forestry. *J. Sustain. For.* **2026**, *45*, 1–30. [CrossRef]
2. Abdullahi, I.U.; Zhang, W.; Cao, Y.; Irankunda, G. Integrating IoT Technology for Fire Risk Monitoring and Assessment in Residential Building Design. *Buildings* **2025**, *15*, 1346. [CrossRef]
3. Wangyel, S.W.; Hee, C.L.; Kyun, W.L. A review of forest fire and policy response for resilient adaptation under changing climate in the Eastern Himalayan region. *For. Sci. Technol.* **2021**, *17*, 180–188. [CrossRef]
4. Luo, Y.X.; Li, Q.; Jiang, L.R.; Zhou, Y.H. Analysis of Chinese Fire Statistics during the period 1997–2017. *Fire Saf. J.* **2021**, *125*, 103400. [CrossRef]
5. Arvan, M.; Givehchi, S.; Rokhsati, S. Identification and prioritization of effective factors in fire incidents preparation programs. *Int. J. Hum. Cap. Urban Manag.* **2016**, *1*, 133–140. [CrossRef]
6. Dubey, S.R.; Jalal, A.S. Fruit and vegetable recognition by fusing colour and texture features of the image using machine learning. *Int. J. Appl. Pattern Recognit.* **2015**, *2*, 160–181. [CrossRef]
7. Kumar, R.; Rutu, S.; Sandeep, B.; Shashank, M. Analysis of Image and Video Using Color, Texture and Shape Features for Object Identification. *IOSR J. Comput. Eng.* **2014**, *16*, 29–33. [CrossRef]
8. Buriboev, S.A.; Abduvait, A.; Jeon, S.H. Integrating Color and Contour Analysis with Deep Learning for Robust Fire and Smoke Detection. *Sensors* **2025**, *25*, 2044. [CrossRef]
9. Zhao, L.; Liu, J.; Peters, S.; Li, J.; Oliver, S.; Mueller, N. Investigating the Impact of Using IR Bands on Early Fire Smoke Detection from Landsat Imagery with a Lightweight CNN Model. *Remote Sens.* **2022**, *14*, 3047. [CrossRef]
10. Ghali, R.; Akhloufi, A.M. Deep Learning Approach for Wildland Fire Recognition Using RGB and Thermal Infrared Aerial Image. *Fire* **2024**, *7*, 343. [CrossRef]
11. Kim, S.; Yang, H.; Cho, K.; Han, K.; Ahn, Y.; Ryu, J.H.; Lee, K. LED array-based multi-angle light scattering for aspirating smoke detection and classification. *Sci. Rep.* **2025**, *15*, 25752. [CrossRef]
12. Ghali, R.; Akhloufi, A.M. BoucaNet: A CNN-Transformer for Smoke Recognition on Remote Sensing Satellite Images. *Fire* **2023**, *6*, 455. [CrossRef]
13. Gragnaniello, D.; Greco, A.; Sansone, C.; Vento, B. Fire and smoke detection from videos: A literature review under a novel taxonomy. *Expert Syst. Appl.* **2024**, *255*, 124783. [CrossRef]
14. Hoang, H.V.; Lee, W.J.; Park, S.C. Enhancing Fire Detection with YOLO Models: A Bayesian Hyperparameter Tuning Approach. *Comput. Mater. Contin.* **2025**, *83*, 4097–4116. [CrossRef]
15. Drzymała, J.A.; Korzeniewska, E. Application of the YOLO algorithm in fire and smoke detection systems for early detection of forest fires in real time. *Przegląd Elektrotechniczny* **2025**, *2*, 44–47. [CrossRef]
16. Ejaz, U.; Hamza, A.M.; Kim, C.H. Channel Attention for Fire and Smoke Detection: Impact of Augmentation, Color Spaces, and Adversarial Attacks. *Sensors* **2025**, *25*, 1140. [CrossRef] [PubMed]
17. Xing, Z.M.; Li, L.Y.; Luo, T.Q.; Liu, X.; Liu, X.; Li, S. Design and Implementation of a Flame and Smoke Detection System Based on Deep Learning. *Heilongjiang Sci.* **2025**, *16*, 135–137. [CrossRef]
18. Verma, P.; Bakthula, R. Empowering fire and smoke detection in smart monitoring through deep learning fusion. *Int. J. Inf. Technol.* **2024**, *16*, 345–352. [CrossRef]
19. Apostolopoulos, I.D.; Athanasoula, I.; Tzani, M.; Groumpos, P.P. An Explainable Deep Learning Framework for Detecting and Localising Smoke and Fire Incidents: Evaluation of Grad-CAM++ and LIME. *Mach. Learn. Knowl. Extr.* **2022**, *4*, 1124–1135. [CrossRef]
20. Han, Y.; Tao, J.; Wang, P.; Shen, Y.; Jiang, H. TriFireNet: A multi-stage framework for robust real-time fire and smoke detection. *J. Saf. Sci. Resil.* **2025**, *6*, 100211.
21. Samy, S.S.; Swarup, Y.S.; Kumar, T.S.; Shankar, C.L.M.; Reddy, S.K.P.; Sudarsan, J.S.; Nithiyanantham, S. Fire and smoke detection using adoption of machine learning algorithm for improving fire safety and disaster preparedness. *Asian J. Civ. Eng.* **2025**, *26*, 3115–3129. [CrossRef]
22. Kwak, D.K.; Ryu, J.K. A Study on the Dynamic Image-Based Dark Channel Prior and Smoke Detection Using Deep Learning. *J. Electr. Eng. Technol.* **2021**, *17*, 581–589. [CrossRef]
23. Chen, C.; Liu, Y.; Zhang, C.; Li, J.; Chen, X. An efficient multi-task forest fire and smoke detection model. *Eng. Appl. Artif. Intell.* **2025**, *160*, 111958. [CrossRef]
24. Khanam, R.; Hussain, M. YOLOv11: An Overview of the Key Architectural Enhancements. *arXiv* **2024**, arXiv:2410.17725. [CrossRef]
25. Ko, B.C.; Kwak, J.; Nam, J. Wildfire smoke detection using temporospatial features and random forest classifiers. *Opt. Eng.* **2012**, *51*, 17208. [CrossRef]
26. Sun, J.; Content, A.; Sun, P. Quantity Representation and Weber-Fechner Law: Applications and Developments. *Psychol. Res.* **2017**, *10*, 35–39. [CrossRef]

27. He, K.M.; Sun, J.; Tang, X.O. Guided Image Filtering. *IEEE Trans. Pattern Anal. Mach. Intell.* **2013**, *35*, 1397–1409. [CrossRef]
28. Binhi, V.N. Magnetic Navigation in Animals, Visual Contrast Sensitivity and the Weber–Fechner Law. *Neurosci. Behav. Physiol.* **2023**, *53*, 1036–1046. [CrossRef]
29. Alwakid, G.; Gouda, W.; Humayun, M. Deep Learning-Based Prediction of Diabetic Retinopathy Using CLAHE and ESRGAN for Enhancement. *Healthcare* **2023**, *11*, 863. [CrossRef]
30. Alkhammash, E.H. A Comparative Analysis of YOLOv9, YOLOv10, YOLOv11 for Smoke and Fire Detection. *Fire* **2025**, *8*, 26. [CrossRef]
31. Liu, L.J.; Chen, S.N. A Real-Time Smoke Detection Model Based on Improved SSD. *J. Xinyang Norm. Univ. (Nat. Sci. Ed.)* **2020**, *33*, 305–311. [CrossRef]
32. Yuan, W.W.; Jiang, S.H.; Shi, C.H. Research on Forest Fire Smoke Recognition Based on Improved GMM Algorithm. *Fire Sci.* **2019**, *28*, 149–155. [CrossRef]
33. Dey, M. Assuring fire safety in nuclear plants with international standards. *Nucl. Eng. Des.* **2024**, *428*, 113532. [CrossRef]
34. Ju, B. A high-reliability edge-side mobile terminal shared computing architecture based on task triple-stage full-cycle monitoring. *IEEE Internet Things J.* **2024**, *10*, 20149–20161. [CrossRef]

Disclaimer/Publisher's Note: The statements, opinions and data contained in all publications are solely those of the individual author(s) and contributor(s) and not of MDPI and/or the editor(s). MDPI and/or the editor(s) disclaim responsibility for any injury to people or property resulting from any ideas, methods, instructions or products referred to in the content.